REDISTRIBUTION OF ALLOYING ELEMENTS DURING TEMPERING OF A NANOCRYSTALLINE STEEL

F.G. Caballero[1], M.K. Miller[2], C. Garcia-Mateo[1], C. Capdevila[1], and S.S. Babu[3]

[1] Centro Nacional de Investigaciones Metalúrgicas (CENIM-CSIC);
Avda Gregorio del Amo, 8; Madrid, E-28040, Spain
[2] Oak Ridge National Laboratory (ORNL), Materials Science and Technology Division;
P.O. Box 2008, Oak Ridge, TN 37831-6136, USA
[3] Edison Welding Institute, Technical Division;
1250 Arthur E Adams Drive, Columbus, Ohio 43221-3585, USA

Keywords: Tempering, atom-probe field-ion microscopy (AP-FIM), bainitic steels, phase transformations

Abstract

Redistribution of alloying elements during tempering of a novel nanocrystalline steel consisting of a mixture of lower bainitic ferrite and carbon-enriched retained austenite has been analysed by atom probe tomography. Three physical processes, namely redistribution of substitutional solute across the austenite/bainitic ferrite interface before retained austenite decomposition, redistribution of solute across the lower bainite cementite/ferrite interface and the precipitation of transition carbides and cementite, have been observed. Results suggest that retained austenite decomposes during tempering before full equilibrium is reached at the interface. Moreover, cementite precipitates from supersaturated ferrite via a paraequilibrium transformation mechanism.

Introduction

It is possible to create bainite in the form of long, slender crystals of ferrite whose scale compares with that of carbon nanotubes [1]. These crystals are approximately 20 nm in thickness and are generated by the partial transformation of austenite at low temperature. The result is an extraordinary combination of strength and toughness as well as the highest hardness ever reported for a bainitic microstructure [2,3]. The transformation mechanism leads to a ferrite carbon concentration, which is many orders of magnitude greater than its equilibrium solubility [1]. Atom probe tomography revealed that this excess of carbon was trapped at dislocations in the vicinity of the ferrite/austenite interface. As a result, decarburization of supersaturated bainitic ferrite and subsequent carbide precipitation sequences are modified [4]. Further studies have shown that the cementite is similar to the one found in lower bainite despite the high silicon content of the steel used. This result confirmed that ε-carbide is not always a precursor to the precipitation of cementite in lower bainite [5]. Moreover, the growth of cementite in lower bainitic microstructure is not associated with partitioning of substitutional elements, including silicon. The above results were explained in terms of a displacive mechanism with paraequilibrium i.e. a homogeneous deformation of supersaturated ferrite combined with the necessary diffusion of carbon [6] by which the cementite lattice is generated. There are many observations that reveal that lower bainitic cementite nucleates and grows within supersaturated ferrite in a process identical to the tempering of martensite [7]. Silicon is known to retard the formation of cementite during the tempering of martensite. Owen [8]

proposed that silicon rejected from cementite acts as a growth barrier and causes the inhibition of cementite precipitation. Since then, partitioning of silicon between cementite and ferrite has attracted considerable attention. Sato and Nishizawa [9] measured the silicon content of cementite equilibrated with ferrite in the Fe-Si-C ternary system at 700 ºC and reported that most of the silicon was rejected from cementite. However, Babu et al. [10] and Thomson and Miller [11] found that there was no initial partition of silicon between ferrite and cementite in tempered martensite of Fe-0.15C-2Si-3Mn and Fe-(0.15, 0.4)C-2.2Cr-1Mo-0.3Si-0.5Mn alloy. Silicon is eventually rejected from cementite during prolonged tempering.

However, a systematic study of the partitioning between ferrite and austenite and also carbide precipitation during tempering of bainite has not been done. There are important differences in the tempering behavior of bainite and martensite. Much of the carbon precipitates as carbides or partitions from the ferrite to the remaining austenite during bainite formation. As a consequence the bainitic microstructure is less sensitive to additional tempering heat treatment. In contrast, the level of carbon in the bainitic ferrite of this novel bainitic steel is unusually high. Previous work focussed on carbon atom redistribution processes, such as segregation of carbon atoms to defects and carbon enrichment in the retained austenite, that occur during auto-tempering conditions [4]. The goals of this work are to analyse the following physical processes:

- Substitutional and interstitial element redistribution between ferrite and austenite
- Redistribution of solute across the lower bainite cementite/ferrite interface
- Precipitation of carbides within the ferrite

Experimental Procedure

The chemical composition of the steel studied is given in Table 1. The alloy was supplied as a cast ingot, samples of which were then homogenized at 1200 ºC for 48 h in partially evacuated sealed quartz capsules that were flushed with argon. The sealed samples were cooled in air following the homogenization heat treatment. Homogenized specimens were austenitized for 15 min. at 1000 ºC, and then isothermally transformed at 200 ºC for 10 days before quenching into water. The microstructure thus obtained was tempered between 400 ºC and 600 ºC during 30 or 60 min.

Transmission electron microscopy (TEM) was used to characterise the original microstructure of the steel and its evolution during tempering. For this purpose, specimens were machined to 3 mm diameter rods and electropolished with a twin-jet electropolisher at room temperature in a mixture of 5 % perchloric acid, 15 % glycerol and 80 % methanol at 40 V until perforation occurred.

X-ray experiments were conducted on etched samples using a Philips PPW1730 diffractometer and a scanning rate of 0.1º min^{-1} over the range 2θ= 30-110º, with unfiltered Cu K_α radiation. The system was operating at 45 kV and 45mA. Peak positions and widths of Bragg reflections were determined by a self-consistent profile-fitting technique using the Pearson-VII function [12]. Retained austenite volume fraction in the microstructure was evaluated by the integrated intensities of the 111, 200, 220 and 311 austenite peaks and the 110, 002, 112 and 022 peaks of ferrite. Using this number of peaks avoids possible bias due to crystallographic texture. Moreover, austenite and ferrite carbon content was calculated from the measured lattice parameters [13-15].

Atom probe tomography specimens were cut from heat treated material and electropolished using the standard double layer and micropolishing methods [16]. Atom probe analyses were performed in the ORNL local electrode atom probe. The large field of view and rapid analysis capability of this instrument facilitated the analysis at an atomic scale in this material. The local

electrode atom probe was operated with a specimen temperature of 60K, a pulse repetition rate of 200 kHz, and a pulse fraction of 0.2.

Results and Discussion

Microstructural evolution during tempering

The initial microstructure is the result of isothermal decomposition of austenite at 200ºC during 10 days. A transmission electron micrograph of the resulting microstructure consisting of fine plates of bainitic ferrite separated by carbon-enriched regions of retained austenite (29 ± 2 % according to X-ray analysis) is shown in Fig. 1a. The retained austenite is sufficiently enriched with carbon (6.69 ± 0.44 at.%), that it remains stable during cooling to ambient temperature, thus martensite does not form at all. The thickness of the bainite plates measured from a selection of transmission electron micrographs is extremely fine, 35 ± 2 nm, which is the main reason for the high hardness value resulting from this microstructure (617 HV) [1]. It is important to point out the high carbon content of the ferrite (2.52 ± 0.30 at.%) as well as the high dislocation density present in this phase, as shown in Fig. 1.a. Carbide particles within bainitic ferrite plates were not observed by TEM; however, cementite precipitated inside bainitic ferrite (i.e. lower bainite cementite) was identified in the initial microstructure by atom probe tomography. More details on the characterisation of this initial microstructure are summarized elsewhere [1,4].

Tempering for 1 h at 400 ºC did not change the hardness (619 HV), suggesting negligible change in the initial microstructure. Extremely fine plates of ferrite and thin films of retained austenite were still observed (see Fig. 1b). The austenite volume fraction also did not change (29 ± 1 %). Only a few carbide particles seem to precipitate within the ferrite. At 450 ºC for 30 min (Fig. 1.c), some of the retained austenite has decomposed into cementite and ferrite. This discrete precipitation would explain a small increase in hardness (up to ~670 HV). The volume fraction of austenite according to X-ray analysis decreased from 29 ± 1 % to 2 ± 1 %. It is also evident (Fig. 1c) that the ferrite plate thickness has not changed, although recovery of dislocation substructure occurs to some extent. Similar microstructural changes are observed when increasing tempering temperatures to 500 or 550 ºC (Figs. 1d and e). Hardness is maintained at high levels (between 615 and 640 HV) and some recovery of dislocations takes place. Ferrite plate thickness increases to 49 ± 2 nm following tempering at 550 ºC for 1 h. Further decomposition of retained austenite occurs as temperature increases, and some large regions of retained austenite transform into colonies of pearlite with a fine interlamellar spacing, Fig. 1e. By contrast, the films of retained austenite decompose into discrete particles of cementite and ferrite because there is insufficient volume to establish the cooperative growth of pearlite [17]. Ferrite plate morphology still remains. Finally, there is a significant reduction in hardness to ~100 HV after 30 min. at 600 ºC due to coarsening of the microstructure, as shown in Fig. 1f.

Redistribution of alloying elements during tempering

It is of interest to evaluate the maximum extent of alloying element partitioning during tempering of low temperature bainite. This was evaluated with thermodynamic calculations and atom probe tomography.

Thermodynamic calculations.- Thermodynamic calculations were performed using the MTDATA computer program [18] in which the equilibria in multicomponent, multiphase systems are determined using critically assessed thermodynamic data. The program was used in conjunction with the SGSOL-SGTE (Scientific Group Thermodata Europe database) Solution Database 3.0. The calculations allowed for inclusion of all the major elements in the bulk alloy, and the phases cementite, M_7C_3, M_6C, $M_{23}C_6$, M_2C, austenite and ferrite. Calculation of the equilibrium microstructures predicted for the steel used in this study that, ferrite, cementite and M_7C_3 were the stable phases at temperatures ranging from 400 to 550 ºC. According to these calculations, the volume fraction of M_7C_3 carbides that should form is less than 2% (negligible). In order to calculate the equilibria between cementite and ferrite, only these two phases were allowed to exist in subsequent MTDATA calculations. The predicted concentrations of the phases are presented in Table 2. The calculations revealed that cementite contains more chromium and manganese at lower temperatures, whereas the silicon composition is nearly zero. Likewise, the equilibria between austenite and ferrite were determined (Table 3). Calculations reveal the existence of a miscibility gap for the FCC phase. According to the equilibrium calculations, two different FCC phases may co-exist at the temperature tested. One phase is austenite and the other is a MC type carbide. In the following sections, the experimentally observed alloying element redistributions determined from atom probe tomography will be compared with the thermodynamic calculations.

Solute clusters in bainitic ferrite.- Carbon atom maps and concentration profiles of bainite at the early stages of tempering (400 ºC for 30 min.) reveal the presence of carbon-enriched regions randomly dispersed throughout the ferrite matrix (see Fig. 2). These clusters are ~6 nm thick and have a maximum carbon content of ~14 at.%, much higher than that detected in austenite, but with too low chromium and manganese contents (less than 2 at.%) to be identified as M_6C carbide particles. These features resemble those carbon clusters with a modulated structure consisting of alternating carbon-rich and carbon-poor bands reported for Fe-Ni-C martensite after natural aging [19,20]. Taylor et al [20] attributed the nature of the carbon atom clustering processes to a spinodal decomposition mechanism since the formation of the carbon cluster was found to occur via a continuous increase in composition amplitude, which is characteristic of this kind of mechanism. However, this fluctuation of solute concentration may be also associated with a redistribution of solute to dislocations in bainite [4]. Irrespective of the mechanism, as suggested by Taylor et al., these carbon enriched regions may be gradually replaced by carbide precipitates as the tempering temperature is increased [21].

Redistribution of alloying elements across the retained austenite/bainitic ferrite interface.- Previous works have shown that during the austenite to bainite transformation, partitioning of substitutional elements between ferrite and austenite phases does not occur [22,4]. An example of an austenite-ferrite interface before tempering for a transformation temperature of 200 ºC in the studied steel is shown in Fig. 3. It is important to note the atom probe data reveal the tendency for carbon enriched austenite (5.39 ± 0.18 at. %) and carbon-depleted ferrite (0.62 ± 0.10 at. %), which is consistent with earlier works [22,4]. Quantitative data also confirms the absence of any partitioning of the substitutional elements between the phases involved. The results are fully consistent with a displacive transformation of austenite to bainite [23]: nucleation occurs by a process akin to the dissociation of arrays of dislocations, in which carbon is able to diffuse; and growth is a diffusionless process, but carbon is soon after transformation rejected into the residual austenite. It is clear from the atom probe data that there is no significant segregation of substitutional elements across the austenite-ferrite interface.

Substitutional elements are expected to redistribute as the mixture of bainitic ferrite and retained austenite are tempered. Stark et al. [24] found by field ion microscopy and atom probe tomography that solutes partition before the retained austenite begins to decompose. 3D atom probe results shown in Figs. 4 and 5 illustrate the redistribution of alloying elements across the austenite/bainitic ferrite interface after tempering at 400 and 450 ºC, respectively, for different times. Carbon atom map in Fig. 4 shows an austenite-ferrite interface after tempering at 400 ºC for 1 h. Element concentration profiles across the interface suggest that no partitioning of susbtitutional elements occur after this tempering condition. The carbon content in the austenite (5.16 ± 0.88 at. %) and in the ferrite (0.57 ± 0.35 at. %) are similar to that measured in the initial microstructure (Fig. 3). Results confirm that tempering for 1 h at 400 ºC did not introduce any change in the original microstructure, even at that atomic level.

There is clear evidence for the redistribution of chromium after tempering at 450 ºC. A 3.5 at. % C iso-concentration surface and elemental concentration profiles of an austenite-ferrite interface for the material tempered at 450 ºC for 30 min. is shown in Fig. 5. ε-carbide was also detected within the ferrite. The distinction between ε-carbide (~30 at.% C) and cementite (~25 at.% C) was made based on the carbon concentration. At this stage, retained austenite begins to decompose (i.e. cementite precipitation) and the carbon content in the austenite (3.75 ± 0.95 at. %) decreases. However, apart from carbon, chromium is still the only other solute that partitions across the austenite-bainitic ferrite interface. It is clear from the chromium concentration profile that the chromium spikes at the austenite/bainitic ferrite interface. An elemental spike usually indicates that negligible partitioning local equilibrium (NPLE) is reached at the interface. Although the concentrations of the substitutional elements at the interface might be at their equilibrium levels, the concentration away from the interface will rapidly drop off. There is no clear indication of silicon or manganese partitioning across the austenite-bainitic ferrite interface. The compositional analysis of the austenite/ferrite interface during tempering indicates that retained austenite decomposes before equilibrium is reached at the interface.

Redistribution of alloying elements across the lower bainite cementite/bainitic ferrite interface.- Previous work has shown that cementite precipitation during lower bainite formation occurs without partitioning of substitutional elements, including silicon [4]. However, during the early stages of tempering, substitutional elements will redistribute across the ferrite-cementite interface. The distribution of carbon atoms in Fig. 6 corresponds to a bainitic ferrite plate (carbon-depleted region) surrounded by a retained austenite film (carbon enriched region) after tempering at 400 ºC for 30 min. Likewise, small carbon clusters (~6 nm thick) with a maximum carbon content of ~15 at.% and a cementite particle at the tip of the sample are detected inside the bainitic ferrite. Besides the apparent low carbon concentration of this lower bainite cementite particle, which is similar to results from other research [4,10,19,25], it is also evident that silicon is depleted in the lower bainite cementite but enriched in bainitic ferrite near the interface. By contrast, partitioning of chromium and manganese is not clear; both enrichments at the interface could be considered as normal scatter of the composition data. By increasing the tempering time, the redistribution of solutes is enhanced. Thus, the concentration profiles in Fig. 7 show higher redistribution of chromium and manganese into lower bainite cementite.

Carbide precipitation during tempering.- TEM observations and atom probe tomography data showed that cementite precipitation occurred after tempering at 400 ºC for 1 h (see Figs. 1.b and 8). During the early stages of tempering, cementite particle forms without redistribution of substitutional solutes, as shown in Fig. 8. Neither elemental spikes nor segregation of silicon,

chromium and manganese were observed at the cementite interface. The absence of partitioning and interfacial segregation of substitutional elements strongly suggests that cementite is formed by paraequilibrium growth during the early stage of tempering, contrary to the situation described in Figs. 6 and 7 for lower bainite cementite. Similar results were reported during tempering of low alloy martensitic steels [10,11]. These measurements distinguished cementite particles formed during tempering at low temperatures from those previously formed in lower bainite.

Atom probe results shown in Figs. 8-11 and Table 4 illustrate the transition from paraequilibrium to local equilibrium of the different solutes after extended tempering times. Concentration profiles in Fig. 9 show the initiation of the redistribution of silicon, but there is no evidence for gross redistribution of chromium and manganese after tempering at 450 ºC for 30 min. Silicon, which is not usually found in cementite at equilibrium, is present after short tempering times, and this is in agreement with previous research [10,11,26]. A cementite particle close to austenite during the course of austenite decomposition is shown in Fig. 9. By increasing the tempering temperature to 500 ºC, redistribution of chromium and manganese is enhanced.

The different solute atom maps in Fig. 10 show extensive redistribution of silicon, chromium and manganese into cementite. Moreover, it is clear from the corresponding concentration profiles for one of the cementite particles that both chromium and manganese spike at the cementite/ferrite interface. Both composition profiles illustrate an intermediate redistribution stage between the paraequilibrium growth mode and the attainment of chromium and manganese equilibrium concentration at the interface (see Table 2). On the other hand, a higher silicon content detected at the centre of cementite particles confirms that silicon partitioning did not take place at the initial stage of cementite formation.

After tempering for 1 h at 550 ºC (Fig. 11 and Table 4), there is virtually no silicon left in the cementite, indicating that silicon has quickly diffused out of the carbide and equilibrium at the cementite/ferrite interface is reached (Table 2). However, chromium and manganese spikes are still evident at this interface. Further tempering is necessary to reach partitioning local equilibrium (PLE) condition (7.20 at.% Cr and 8.45 at.% Mn according to calculation in Table 2). By contrast, the previously [10] measured nominal concentrations of silicon and manganese in ferrite and cementite after various tempering heat treatments showed that the redistribution of manganese into cementite occurred faster than that of silicon into ferrite for a steel with a nominal silicon alloy concentration of 3.84 at.% and a nominal manganese alloy concentration of 2.95 at.%.

The ε-carbide was not found as a precursor to the precipitation of cementite in lower bainite in the studied steel [4]. However, ε-carbide was detected by atom probe tomography for different tempering conditions. Chang and Smith [27] have previously shown that ε-carbide precipitation did not accompany the partitioning of substitutional elements during the early stage tempering. They showed that there was no enrichment of silicon in the ε-carbide. The extensive atom probe tomography results presented herein failed to detect ε-carbide at tempering temperatures lower than 450 ºC. Atom probe results for a sample tempered at 450 ºC for 30 min. are shown in Fig. 5. The carbon concentration in the particle at the right bottom corner of the 3.5 at.% iso-concentration surface is ~30 at.%, which is consistent with the carbides being ε-carbide. At this stage of tempering, significant depletion of silicon from ε-carbide is observed, whereas chromium and manganese are slightly enriched within the ε-carbide. The same conclusions are achieved when the ratio of iron to substitutional solute atoms as a function of distance is represented. Further tempering enhances the redistribution of chromium and manganese, as

illustrated in the concentration profiles across the ε-carbide shown in Fig. 10. These results are in agreement with previous research [27-29].

These results indicate a complex transition of a starting, nonequilibrium microstructure to its equilibrium state during tempering. Thermodynamic calculations indicated that this steel will have ferrite and cementite under thermodynamic equilibrium. However, the experimental measurements indicate a myriad of intermediate microstructures and phase formation. The intermediate microstructures are summarized in a schematic illustration (see Fig. 12). These results indicate that there is no unique path for the equilibration process for the steel studied here. Often these intermediate phase transformations may be associated with changes in tempering kinetics. The enhanced temper resistance of these steels may be attributed to multiple paths for the transition of the microstructure during the equilibration process [1].

Conclusions

A local electrode atom probe has been used to analyse the atomic redistribution processes that take place during tempering of a novel nanocrystalline bainitic steel. The compositional analysis of the austenite/ferrite interface indicates that retained austenite decomposes during tempering before equilibrium is reached at the interface. Moreover, significant fluctuation of the carbon concentration, randomly dispersed throughout a carbon depleted ferrite matrix, was observed at the early stages of tempering. It is likely that these carbon enriched regions may signify the onset of transitional carbide precipitation.

On the other hand, no partitioning of substitutional solutes was observed between cementite and ferrite after tempering at 400 ºC for 1 h. By increasing the temperature/time, concentration profiles show a gradual change toward equilibrium concentrations at the cementite/ferrite interface. Silicon diffused out of the carbide, reaching an equilibrium concentration at the cementite/ferrite interface. However, the presence of chromium and manganese spikes at the cementite/ferrite interface indicates that negligible partitioning local equilibrium (NPLE) is reached at the interface.

The results indicate that there is no unique path from a nonequilibrium to an equilibrium microstructure in these steels, which likely leads to enhanced tempering resistance.

Acknowledgement

The authors acknowledge financial support from European Coal and Steel Community (ECSC 7210-PR-345) and Spanish Ministerio de Ciencia y Tecnología (Project-2006 6 0I 029). CGM would also like to thank Spanish Ministerio de Ciencia y Tecnología for the financial support in the form of a Ramón y Cajal contract (Programa RyC 2004). Research at the Oak Ridge National Laboratory SHaRE User Facility was sponsored by the Office of Basic Energy Sciences, Division of Scientific User Facilities, U.S. Department of Energy, under contract DE-AC05-00OR22725 with UT-Battelle, LLC. Authors also would like to express their special acknowledgement to Prof. H.K.D.H. Bhadeshia for helpful discussions.

References

1. Caballero FG, Bhadeshia HKDH. Curr Opin Solid St M 2004; 8: 251
2. Garcia-Mateo C, Caballero FG. Mater Trans 2005; 46: 1839
3. Garcia-Mateo C, Caballero FG. ISIJ Int 2005; 45: 1736
4. Caballero FG, Miller MK, Babu SS, Garcia-Mateo C. Acta Mater 2007; 55: 381
5. Bhadeshia HKDH, Edmonds DV. Metall Trans 1979; 10A: 895

6. Yakel HC. Int Met Rev 1985; 30: 17
7. Bhadeshia HKDH. Acta Mater 1980; 28: 1103
8. Owen WS. Trans ASM 1954; 46: 812
9. Sato T, Nishizawa T. J Jpn Inst Met 1955; 19: 385
10. Babu SS, Hono K, Sakurai T. Metall Mater Trans 1994; 25A: 499
11. Thomson RC, Miller MK. Acta Mater 1998; 46: 2203
12. Langford J, Lourer D. Rept Prog Phys 1996; 59: 131
13. Dyson DJ, Holmes B. Journal of the Iron and Steel Institute 1970; May: 469
14. Bhadeshia HKDH, David SA, Vitek JM, Reed RW. Mater Sci Tech 1991; 7: 686
15. Cullity BD, Stock SR. Elements of X-ray diffraction. 3rd edition. Prentice Hall, Upper Saddle River, 2001, p. 411.
16. Miller MK. Atom Probe Tomography. Kluwer Academic/Plenum Press (NY), 2000. p.28.
17. Yang JR, Bhadeshia HKDH. Mat Sci Eng 1991; A131: 99
18. MTDATA: Phase diagram calculation software. National, Physical Laboratory, Teddington, 2003.
19. Miller MK, Beaven PA, Smith GDW. Metall Mater Trans 1981; 12A: 1187
20. Taylor KA, Chang L, Olson GB, Smith GDW, Cohen M, Van der Sande JB. Metall Mater Trans 1989; 20A: 2717
21. Taylor KA, Olson GB, Cohen M, Van der Sande JB. Metall Mater Trans 1989; 20A: 2749
22. Bhadeshia HKDH, Waugh AR. Acta Metall 1982; 30: 775
23. Bhadeshia HKDH, Edmonds DV. Acta Metall 1980; 28: 1265
24. Stark I, Smith GDW, Bhadeshia HKDH. Metall Mater Trans 1990; 21A: 847
25. Sha W, Smith GDW. Surf Sci 1992; 266: 416
26. Babu SS, Hono K, Sakurai T. Appl Surf Sci 1993; 67: 321.
27. Chang L, Smith GDW. J Phys 1984; 45: 397.
28. Barnard SJ, Smith GDW, Garratt-Reed AJ, Van der Sande J. In: Aaronson HI, Laughlin DE, Sekerka RF, Wayman CM, editors. Proc. Solid-Solid Phase Transformations. Warrendale (PA): TMS-AIME, 1981. p. 881.
29. Miyamoto G, Furuhara T, Maki T, Oh JC, Hono K. In: Howe JM, Laughlin DE, Lee JK, Dahmen U,. Soffa WA, editors. Proc. Solid-Solid Phase Transformations in Inorganic Materials: Diffusional Transformations, vol. 1. Warrendale (Pennsylvania): The Minerals, Metals and Materials Society, 2005. p. 363.

Table(s)

Tables

Table 1. Chemical Composition

	C	Si	Mn	Mo	Cr	V
wt-%	0.98	1.46	1.89	0.26	1.26	0.09
at. %	4.34	2.76	1.82	0.14	1.28	0.09

Table 2. Concentration of cementite and ferrite in equilibrium from MTDATA, at.%.

Temperature	Phase	C	Cr	Mn	Si	Mo	V	Fe
400 ºC	Cementite	25	7.67	10.24	-	0.05	-	57.04
	Ferrite	-	0.02	0.17	3.33	-	-	96.48
450 ºC	Cementite	25	7.56	9.76	-	0.09	-	57.58
	Ferrite	-	0.04	0.26	3.33	-	-	96.36
500 ºC	Cementite	25	7.40	9.16	-	0.15	0.02	58.27
	Ferrite	-	0.07	0.37	3.33	0.01	-	96.22
550 ºC	Cementite	25	7.20	8.45	-	0.22	0.03	59.00
	Ferrite	-	0.10	0.50	3.33	0.02	-	96.00

Table 3. Concentration of austenite and ferrite in equilibrium from MTDATA, at.%.

Temperature	Phase	C	Cr	Mn	Si	Mo	V	Fe
400 ºC	Austenite	16.71	0.24	4.36	0.35	-	-	78.34
	Ferrite	0.05	-	0.08	3.19	-	-	96.68
	FCC 2*	45.93	19.29	21.72	-	2.19	1.43	9.44
450 ºC	Austenite	14.98	0.43	8.58	0.52	-	-	75.48
	Ferrite	0.05	-	0.31	3.31	-	-	96.32
	FCC 2	46.02	25.44	7.90	-	2.98	1.95	15.72
500 ºC	Austenite	12.47	0.62	7.04	0.85	0.01	-	79.01
	Ferrite	0.06	0.03	0.44	3.40	-	-	96.08
	FCC 2	45.97	28.12	3.06	-	3.46	2.30	17.09
550 ºC	Austenite	10.26	0.91	5.23	1.18	0.02	-	82.40
	Ferrite	0.07	0.09	0.52	3.51	-	-	95.81
	FCC 2	45.18	28.98	1.73	-	4.03	2.78	17.30

*Calculation reveals the existence of a miscibility gap for FCC phase. Two different FCC phases may co-exist at the temperature tested. One of them is austenite and FCC 2 is MC type carbide

Table 4. Measured mean concentration of chromium, manganese and silicon in cementite and ferrite after various tempering heat treatments (See concentration profiles in Figs. 8-11)

Tempering	Phase	Cr, at.%	Mn, at.%	Si, at.%	Mo, at.%	V, at.%
400 ºC / 1 h.	Cementite	1.85±0.37	1.08±0.35	3.14±0.69	0.69±0.30	0.21±0.17
	Ferrite	1.45±0.47	1.24±0.36	3.44±0.80	0.58±0.35	0.14±0.17
450 ºC / 30 min	Cementite	1.64±0.57	0.97±0.44	2.11±1.04	0.50±0.28	0.19±0.18
	Ferrite	1.49±0.86	1.04±0.46	3.38±0.86	0.56±0.34	0.16±0.19
500 ºC / 30 min	Cementite	1.90±0.61	1.03±0.44	0.18±0.30	0.57±0.35	0.26±0.22
	Ferrite	0.57±0.40	0.48±0.38	3.93±1.04	0.40±0.32	0.08±0.14
550 ºC / 1 h.	Cementite	2.86±0.77	1.55±0.53	0.08±0.10	0.48±0.18	0.32±0.14
	Ferrite	0.94±0.36	0.68±0.28	2.99±0.71	0.31±0.19	0.09±0.10

Figures

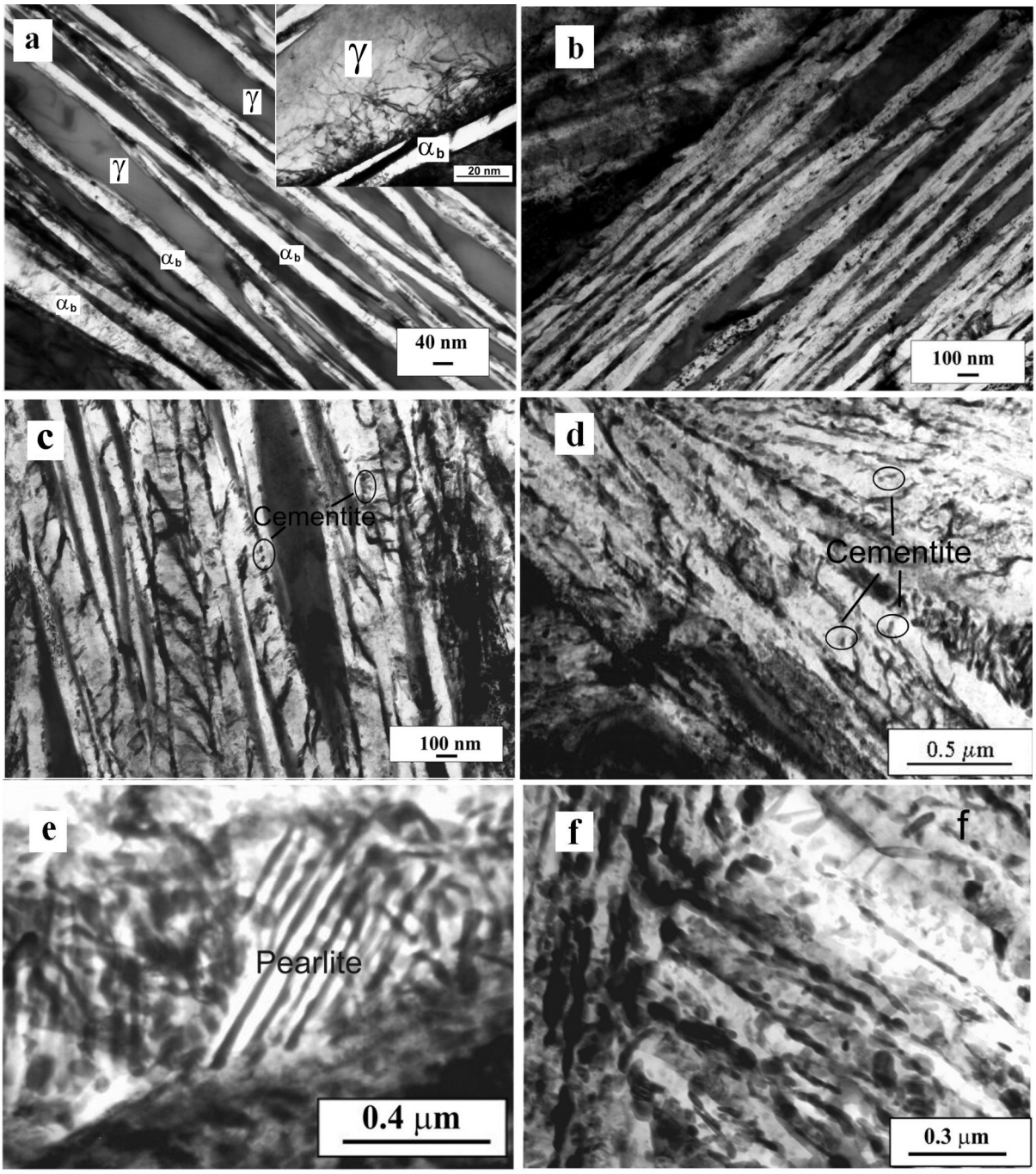

Figure 1.- Evolution of microstructure during tempering. Transmission electron micrographs of (a) initial microstructure; and tempered microstructures at: (b) 400 ºC for 1 h; (c) 450 ºC for 30 min; (d) 500 ºC for 30 min; (e) 550 ºC for 1 h; and (f) 600 ºC for 30 min. α is ferrite and γ is austenite

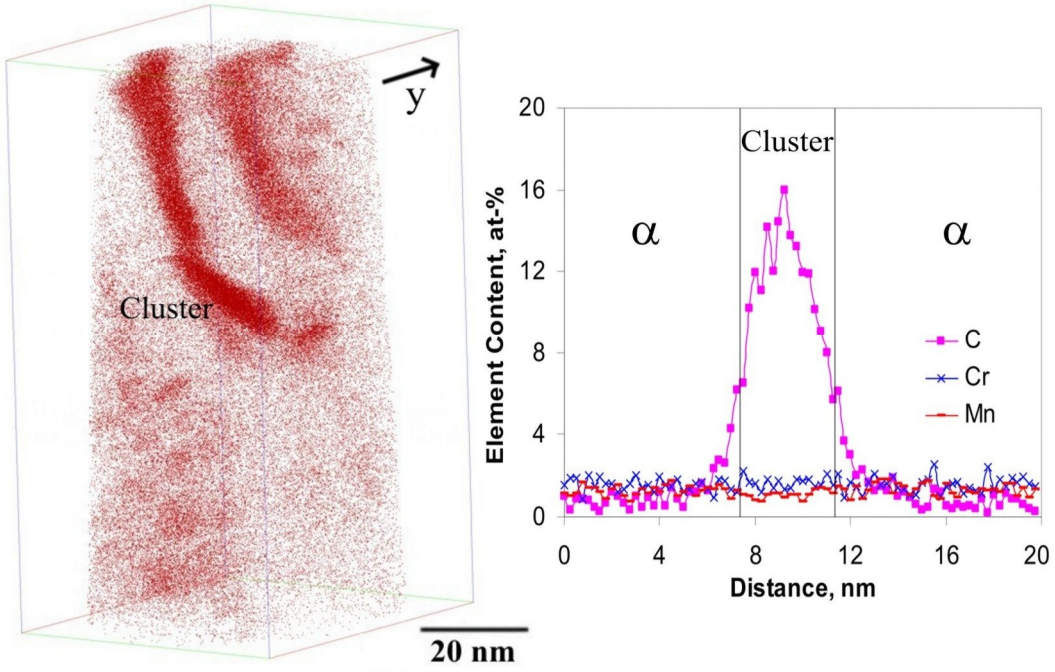

Figure 2.- Carbon atom map and concentration profile along the marked y direction across a carbon cluster in bainitic ferrite after tempering at 400 ºC for 30 min. α is ferrite. Size of the sampling box: 27 nm x 5 nm by 20 nm long.

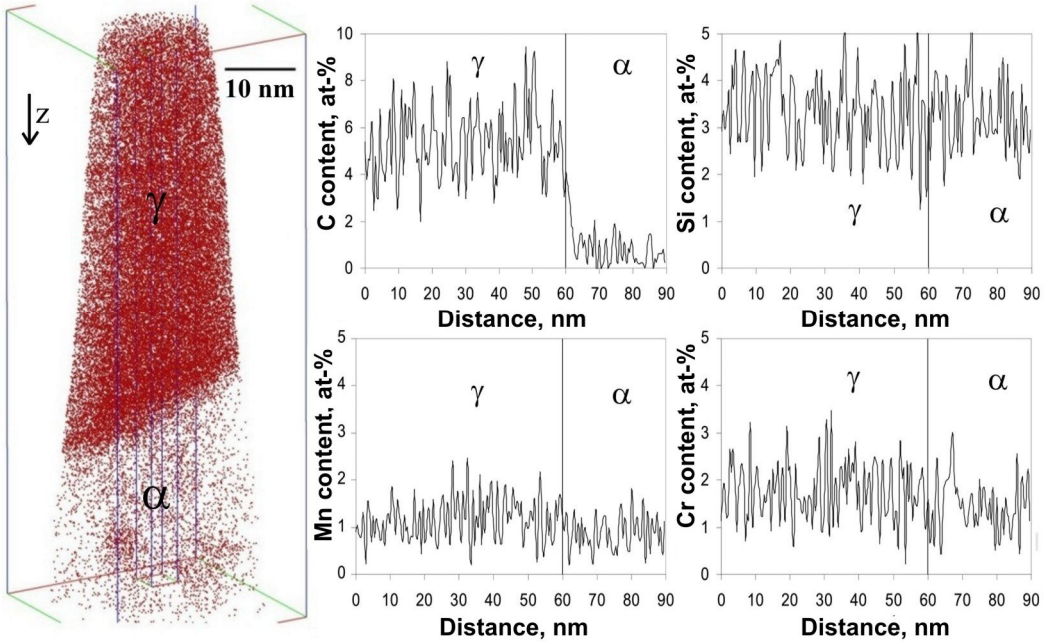

Figure 3.- Carbon atom map and concentration profile along the marked z direction across austenite/bainitic ferrite interface before tempering. α is ferrite and γ is austenite.

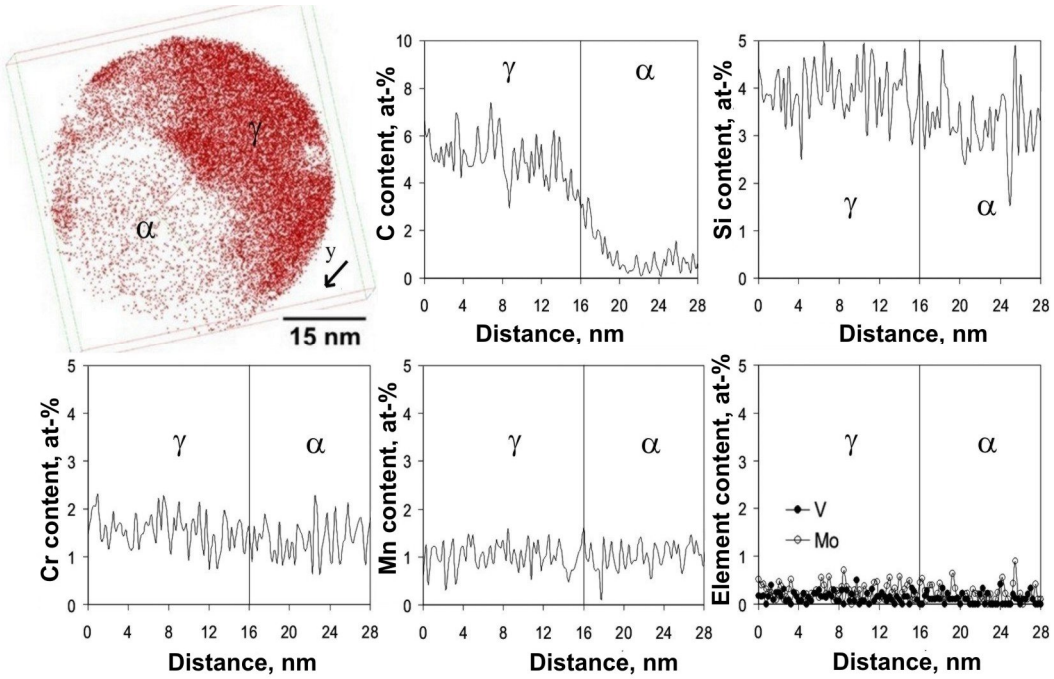

Figure 4.- Carbon atom map and concentration profile along the marked y direction across austenite/bainitic ferrite interface after tempering at 400 ºC for 1 h. α is ferrite and γ is austenite.

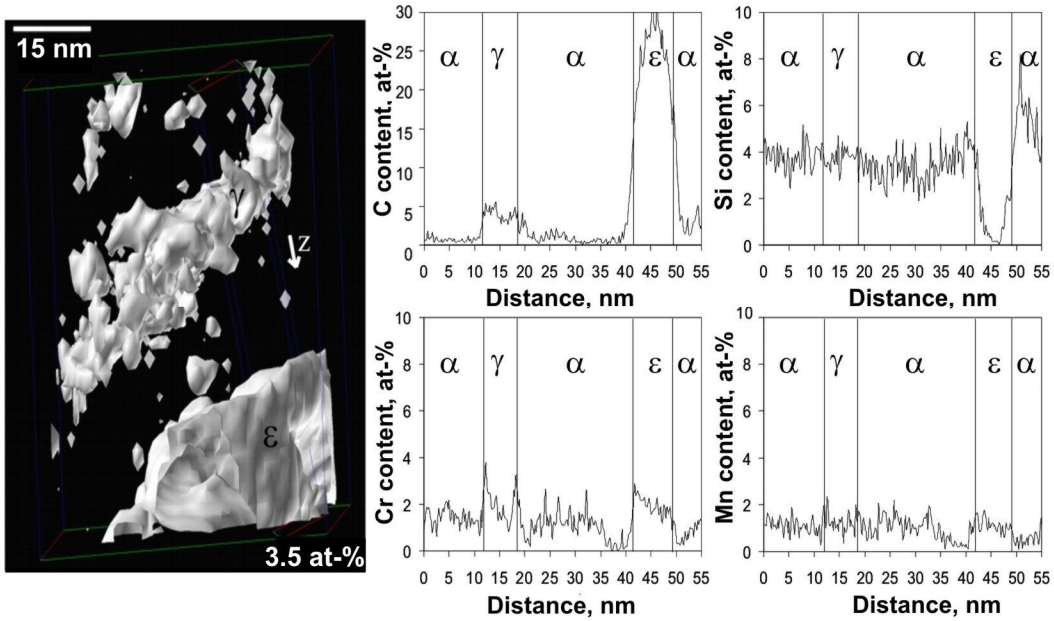

Figure 5.- 3.5 at% carbon iso-concentration surface and concentration profile along the marked z direction across austenite/bainitic ferrite interface after tempering at 450 ºC for 30 min. α is ferrite, γ is austenite and ε is ε-carbide.

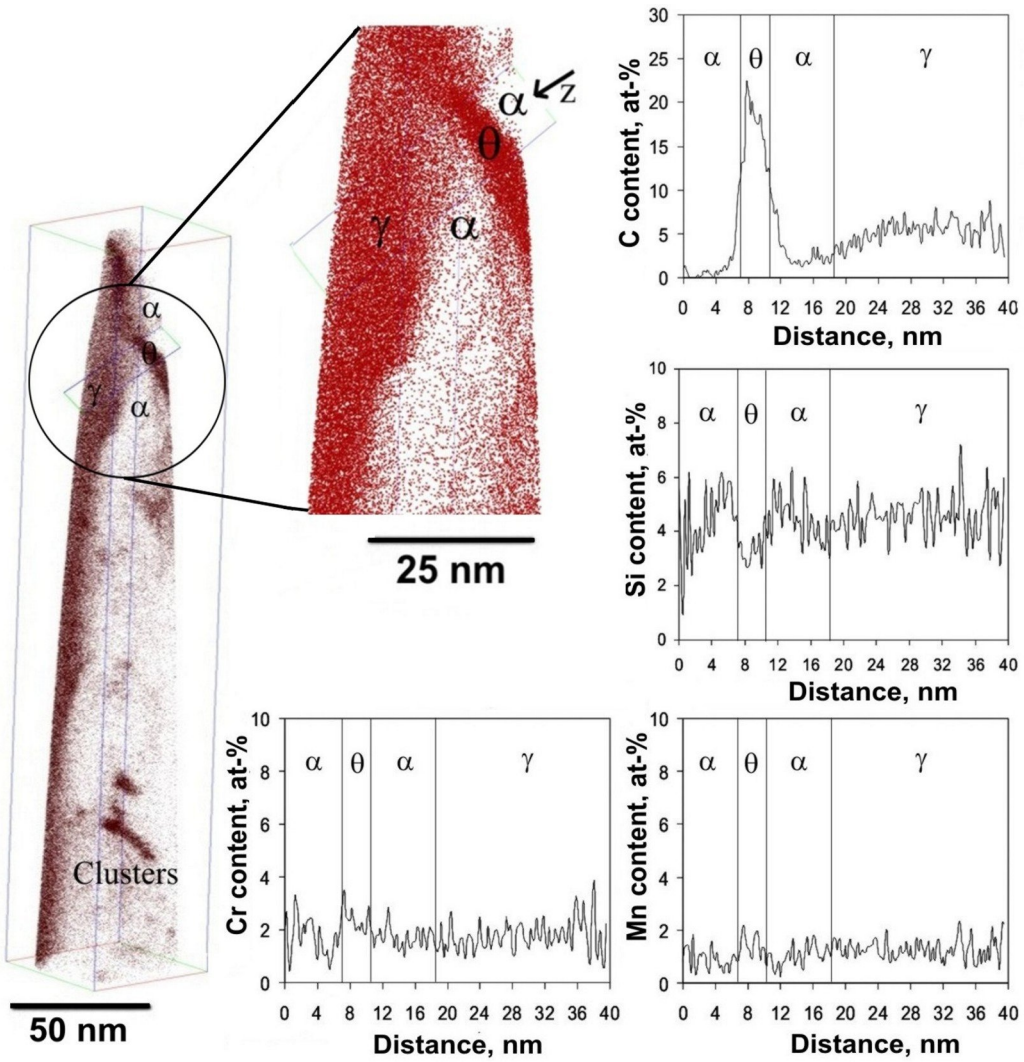

Figure 6.- Carbon atom map and concentration profile along the marked z direction across lower bainite cementite particle after tempering at 400 ºC for 30 min. α is ferrite, γ is austenite and θ is cementite. Region of analysis in atom map has been enlarged in order to show more clearly the features of interest.

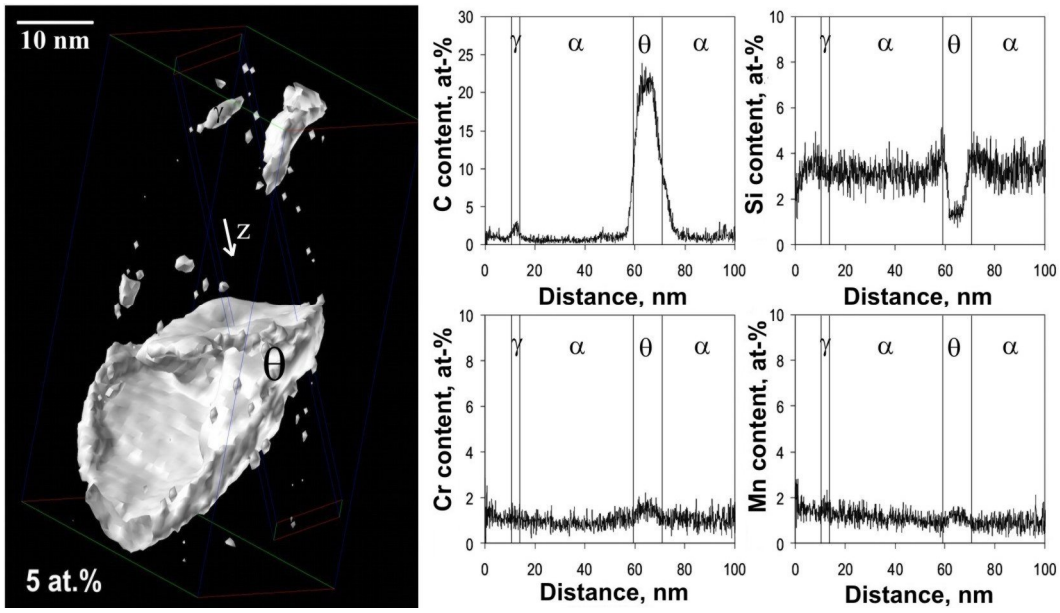

Figure 7.- 5 at.% iso-concentration surface and concentration profile along the marked z direction across lower bainite cementite particle after tempering at 400 ºC for 1 hour. α is ferrite and θ is cementite.

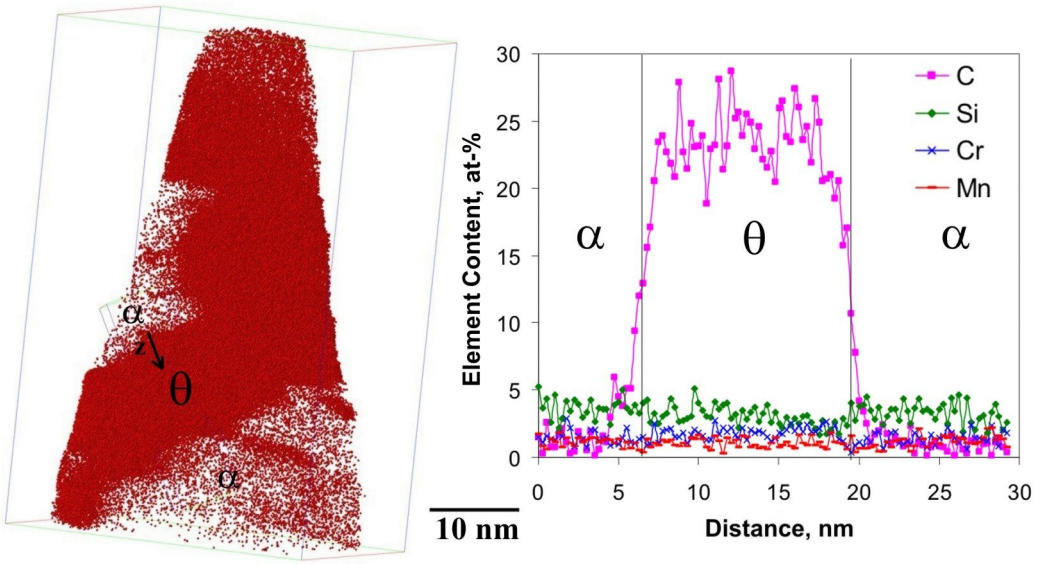

Figure 8.- Carbon atom map and concentration profile along the marked z direction across bainitic ferrite/cementite interface after tempering at 400 ºC for 1 h. α is ferrite and θ is cementite.

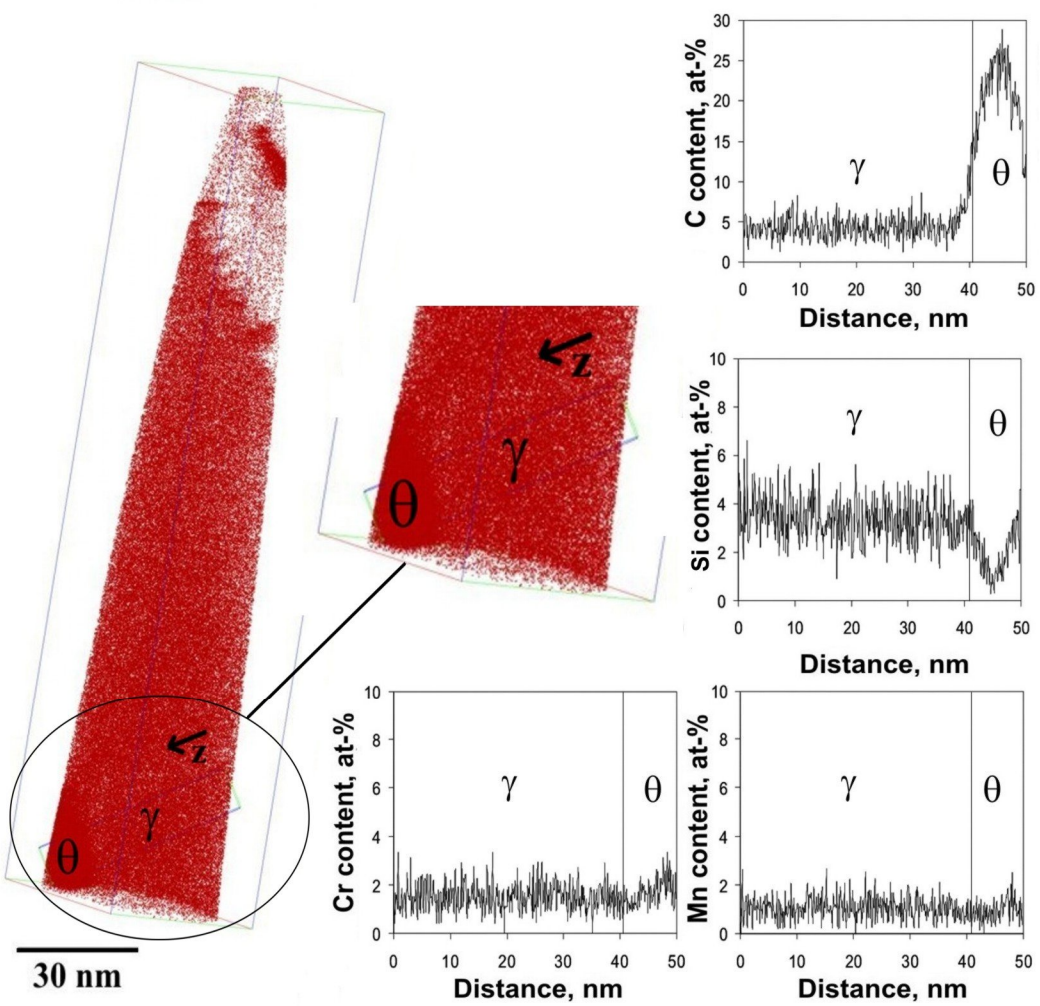

Figure 9.- Carbon atom map and concentration profile along the marked z direction showing cementite precipitation after tempering at 450 ºC for 30 min. γ is ferrite and θ is cementite. Region of analysis in atom map has been enlarged in order to show more clearly the features of interest.

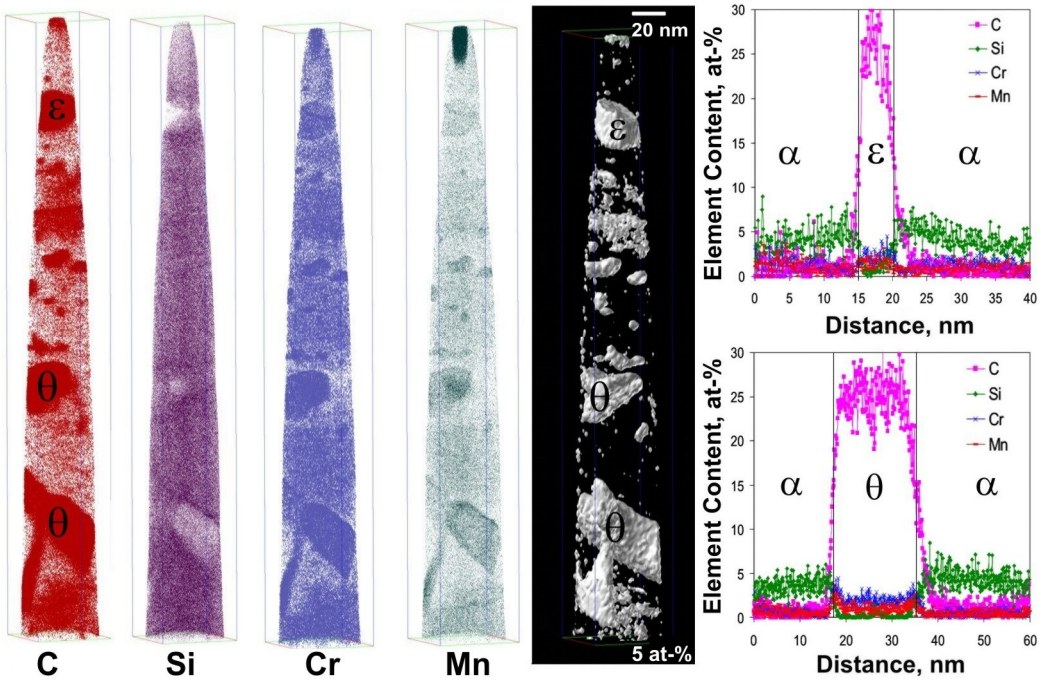

Figure 10.- Solute atom maps, 5 at.% iso-concentration surface and concentration profiles showing carbide particles precipitated after tempering at 500 ºC for 30 min (solute enriched region at the tip is a border artifact). α is ferrite, θ is cementite and ε is ε-carbide.

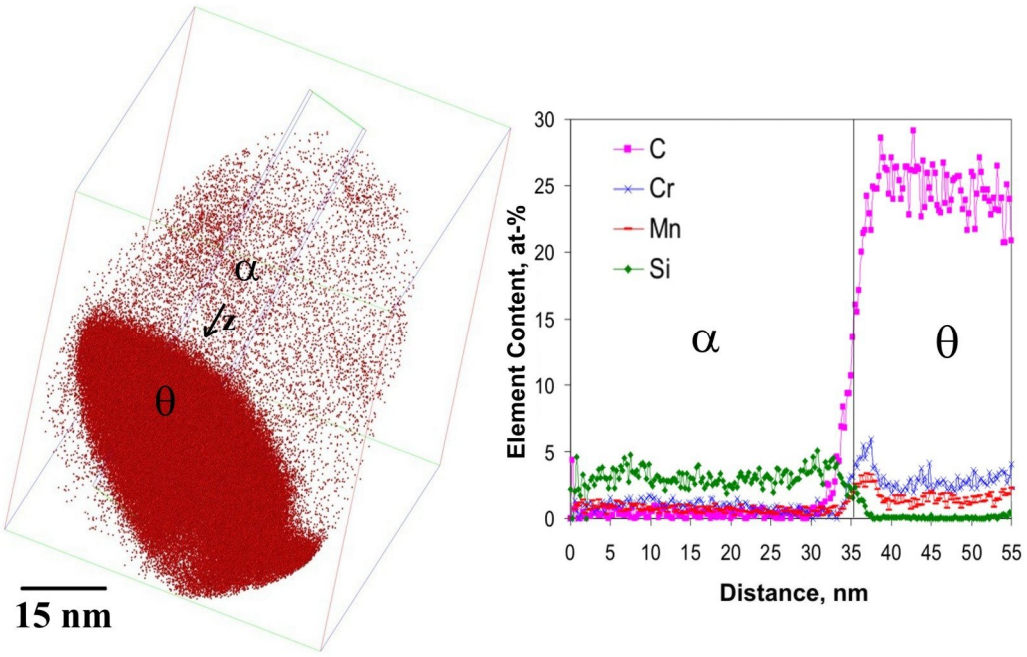

Figure 11.- Carbon atom map and concentration profile along the marked z direction across bainitic ferrite/cementite interface after tempering at 550 ºC for 1 h. α is ferrite and θ is cementite.

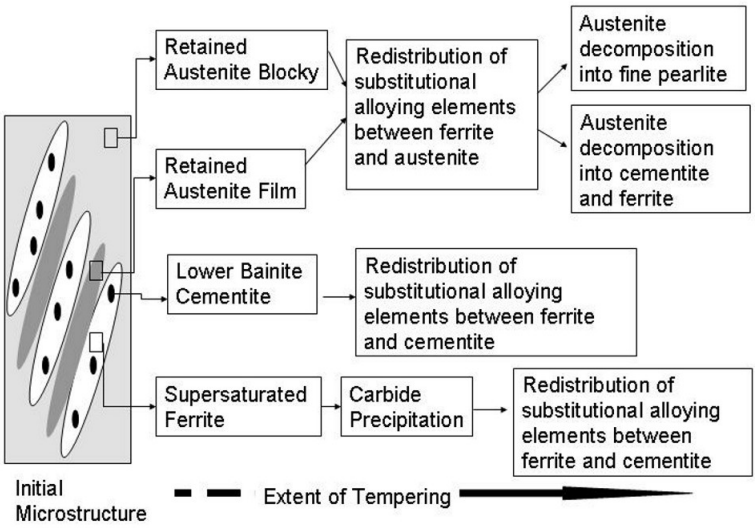

Figure 12.- Transition of microstructures towards an equilibrium state during tempering of the studied steel.